

Femtosecond Photocurrents at the FeRh/Pt Interface

R. Medapalli^{1,2,a),b)}, G. Li³, Sheena K. K. Patel¹, R. V. Mikhaylovskiy^{3,4}, Th. Rasing³,
A. V. Kimmel³, and E. E. Fullerton¹

¹Center for Memory and Recording Research, University of California, San Diego, La Jolla, California
92093-0401, USA

²Department of Physics, School of Sciences, National Institute of Technology, Andhra Pradesh-534102,
India

³Radboud University, Institute for Molecules and Materials, Heyendaalseweg 135, Nijmegen 6525 AJ,
The Netherlands

⁴Department of Physics, Lancaster University, Bailrigg, Lancaster LA1 4YW, UK

- a) The author to whom the correspondence should be addressed
- b) Electronic mail: rajshekhar85@gmail.com

Femtosecond laser excitations of FeRh/Pt bilayers launches an ultrafast pulse of electric photocurrents in the Pt-layer and subsequently results in emission of electromagnetic radiation in the THz spectral range. Analysis of the THz emission as a function of the polarization of the femtosecond laser pulse, external magnetic field, sample temperature and sample orientation shows that the photocurrent can emerge due to vertical spin pumping and photo-induced inverse spin-orbit torque at the FeRh/Pt interface. The vertical spin pumping from FeRh into Pt does not depend on the polarization of light and originates from ultrafast laser-induced demagnetization of the ferromagnetic phase of FeRh. The photo-induced inverse spin-orbit torque at the FeRh/Pt interface can be described in terms of a helicity-dependent effect of circularly polarized light on the magnetization of the ferromagnetic FeRh and the subsequent generation of a photocurrent.

In recent years, there has been increasing interest in antiferromagnetic (AF) materials to dramatically improve spintronics technology in terms of density and speed [1]. Unlike ferromagnets, AF materials produce either no or very small stray fields that would minimize cross-talking between neighboring devices. They further have up to 10^3 higher frequency spin resonances [2], which promises to push the operation frequency of spintronics devices to the THz domain [3]. This is why understanding spin transport in antiferromagnets is emerging as one of the hottest topics in magnetism research.

FeRh is a rather unique AF material as it undergoes a first-order phase transition to ferromagnetic (FM) with increasing temperature. Due to this property, FeRh offers a unique playground to investigate spintronics phenomena across the transition between AF and FM phases in the same material [4,5]. For instance, vertical and lateral spin pumping during the phase transition have been recently reported for FeRh/Pt and FeRh/Py bilayers [6]. Evidence of THz vertical spin currents in FeRh/Pt was obtained with the help of THz emission

spectroscopy in Ref. [7]. Although, several hypotheses inspired by Refs [8,9] have been suggested, the exact origin of the spin currents was not identified. One of the reasons for the difficulties hampering interpretation was the observation of rather different temperature dependencies of the net magnetization, measured by vibrating sample magnetometer, and the amplitude of the laser-induced THz emission. While the magnetization measurements revealed a temperature hysteresis typical for first-order phase transitions, such a temperature hysteresis was not seen in the THz measurements [7].

In this Letter, we resolve this ambiguity, reveal and compare two main spin-dependent sources of the laser-induced THz emission in an FeRh/Pt bilayer. We show that the most intense source does not depend on the polarization of light (helicity-independent), which is evidenced by the THz vertical spin currents and originates from ultrafast laser-induced demagnetization of FM FeRh. Its contribution scales with the amount of the FM phase. The second, weaker, source of THz emission depends on the polarization of light

and is due to a photo-induced tilt of the magnetization and the inverse spin-orbit torque effect at the FeRh/Pt interface.

For our study we chose two different thicknesses for FeRh (20 and 40 nm). First, the FeRh films were deposited via sputter deposition onto MgO(001) single crystals and then the samples were capped with a 5-nm-thick Pt or Au layer. We chose the thickness of heavy-metal layer such that the inverse spin-Hall effect (ISHE) based spin-to-charge conversion is efficient [10,11]. The FeRh was deposited at 450 °C and then post annealed at 800 °C for 45 min to improve the crystalline and chemical order. The Pt layer was deposited at room temperature. The layer thicknesses are found from X-ray reflectometry (see Fig.1a). The observed small period oscillations originate from the full thickness of FeRh/Pt bilayer, and the large period oscillations from the 5-nm Pt layer. The high-quality reflectometry (Fig.1a) and the x-ray diffraction (see Fig. 1b) indicate a smooth film with epitaxial growth of FeRh(001). The presence of FeRh (001) and (003) peaks indicate the chemical ordering in the CsCl-type B2 structure. At 300 K, the lattice along the normal to the film is relaxed leading to compressive strain determined by the MgO substrate that further leads to differences of expansion between the in-plane and out-of-plane directions at the AF-FM phase transition [12].

The AF-FM magnetic phase transition (Fig.1c) was probed by vibrating sample magnetometry showing a clear hysteresis in the phase-transition upon sweeping the sample temperature, reflecting the first-order character of the magnetic phase transition. The transition temperature is 370 K under modest external magnetic field with a 20 K width of the temperature hysteresis showing that within the hysteresis AF and FM phases can co-exist (see Fig.1c). Strain and structurally inhomogeneous defects can broaden the phase transition over the sample, leading to co-existence of AF and FM phases in the transition region. In addition, several groups reported observation of FM-domains at the MgO/FeRh interface at T=300 K, well below the temperature of the phase transition [12-14].

Our experimental approach to photo-excite the FeRh/Pt sample is similar to the one employed in Ref. [7], but included the possibility to change the external magnetic field and apply larger laser fluences (up to ~ 10 mJ/cm²). The schematic of the THz electric field emission spectroscopy

combined with the ultrashort optical excitation is shown in Supplementary Material Fig.S1. The 50-fs optical pulses with a central wavelength of 800 nm, were generated by a pulsed Ti:Sapphire laser with a regenerative amplifier operating at a repetition rate of 1 kHz. A pump pulse was focused onto the sample at normal incidence (z -axis in Fig.1) with a 2-mm-diameter spot size. The polarization of the laser pulse was varied between linear, right- and left-circular polarization using a combination of a polarizer and a quarter wave retarder plate. The positions of the optical components were fixed such that the beam profile and its position on the sample plane would not change while the waveplate is rotated to change the helicity of the pump laser. The magnetization is parallel to the x -axis, and we detect the \hat{x} , and \hat{y} , components of the electric field of the emitted THz radiation propagating along the z -axis. An external magnetic field, B was applied along the x -axis to control the in-plane magnetization. Two opposite directions of the applied external magnetic field along and anti-parallel to the x -axis are denoted as M^+ and M^- , respectively. The THz emission generated from the sample was focused onto a ZnTe crystal by two gold coated parabolic mirrors. The THz electric field was measured by detecting the ellipticity changes of the gating pulse induced by the Pockel's effect in ZnTe using a balance detector in combination with a lock-in amplifier.

Figure 1d (top panel) illustrates laser-induced spin currents and their conversion into charge currents via the ISHE, which produces THz radiation with the electric field transients as depicted. This mechanism is independent of the helicity of the light. Femtosecond laser pulse heats the sample, changes the magnetization of FeRh and photo-excite spin currents from FeRh to Pt. The currents entering the Pt layer have spin polarization along the magnetization of FM phase (M^+ or M^-). In Pt the spin-to-charge conversion takes place due to the ISHE. This mechanism is very similar to the one employed in Ref. [6] to study vertical spin pumping in magnetic/heavy-metal thin film bilayers. The bottom panel image in Fig.1d is the THz emission that depends on the circular polarization of the light. The THz emission arises from helicity-dependent femtosecond laser-induced rotation of the magnetization in the plane of the sample which, due to the inverse spin-orbit torque, generates a femtosecond pulse of electric current at the interface. We made use of wire-grid polarizers to

separately measure the THz emission polarized along the x and y -axes. This gives the opportunity of differentiating the electric field components of helicity-independent (E_y) and $-$ -dependent (E_x) mechanisms. A thermocouple heater was used to vary the temperature of the sample between 300-450K (heating process) or 450-300 K (cooling process).

The time traces of the helicity-independent and helicity-dependent THz electric field components measured at various temperatures are shown in Figs.2a and 2b, respectively. The waveforms corresponding to the dynamics of the (helicity-independent) y -component exhibit identical shapes, with a monotonous change in the amplitude with heating. This suggests that the spectrum of the THz emission and the sub-picosecond dynamics of the helicity-independent spin current does not depend on the relative AF and FM phase contributions. The helicity-dependent electric field component is determined from four combinations of (σ, M) , $E_{x,odd} = (E_x^{(M\uparrow, \sigma+)} - E_x^{(M\uparrow, \sigma-)} - E_x^{(M\downarrow, \sigma+)} + E_x^{(M\downarrow, \sigma-)})/4$, and its corresponding dynamics measured at various temperatures are shown in Fig.2b. The time-traces of the y -component of the pump induced THz electric field emission for two opposite directions of the applied external magnetic field ($B = \pm 150$ mT) measured at 300 K (AF-phase) are shown in Supplementary Material Fig.S2a. The THz frequency ranges up to 3 THz and peaks at 0.75 THz (not shown).

There is a change of sign in the detected THz waveforms upon reversal of the external magnetic field direction. We also pumped the sample from both the substrate-side as well as the Pt-capping side. The corresponding time traces of the THz emission signal are shown in Supplementary Material Fig.S2b. For a given magnetic field direction, a change in sign of the laser-induced THz-signals after rotating the sample by 180° around the x -axis indicates that the emitter of the THz E_y -field is of electric dipole origin [11,25]. The symmetries of the experiments are in full agreement with the mechanism discovered for the Pt/Co bilayers [11], where a sub-picosecond demagnetization of Co launched a vertical spin current across Pt/Co interface and the Pt-layer converted the spin current into a charge current via the ISHE [16]. In our case, the spin current can originate either from magnetization induced in the AF-phase due to an ultrafast phase transition to the FM state [17,18,19], or due to an ultrafast demagnetization

of the FM-domains [20] present in FeRh at higher temperatures or even below the temperature of the phase transition.

The peak value of the detected THz E_y -field components denoted as $\text{Max.}(|E_y|)$ is plotted as a function of temperature for the heating and cooling processes (see Fig.3). For comparison, the static net magnetic moment curves (for both heating and cooling) are shown as dashed lines in Fig.3 as well. Unlike the behavior of the net magnetization, similarly to Ref.[7], the electric field components do not show any temperature hysteresis. The temperature dependency of the peak value of THz $E_{x,odd}$ -component, $\text{Max.}(|E_{x,odd}|)$ is also shown in Fig.3, exhibiting a trend similar to $\text{Max.}(|E_y|)$. Figure 4a shows the $\text{Max.}(|E_y|)$ as a function of the applied magnetic field strength at five different initial temperatures (300, 360, 370, 380, and 450 K). It is seen that the magnetic field hysteresis becomes broader upon temperature increase. The Fourier spectrum of the emitted THz E_y -radiation (see Fig. 4b) does not depend on the applied magnetic field, which shows that the field does not affect the sub-picosecond dynamics of the vertical spin currents across the interface.

The lack of temperature-hysteresis in the THz measurements (see Fig.3) is a result of the stroboscopic nature of the experiment, which implies measurement of the THz electric field averaging over many heating-cooling cycles. From the very beginning of ultrafast magnetism, it is well established that stroboscopic measurements of spin dynamics cannot adequately reveal a temperature hysteresis [26]. More particularly, a temperature-hysteresis implies that in a certain temperature range the medium has multiple stable states. The hysteresis can disappear in stroboscopic measurements, because after the very first pump-induced heating and cooling down every next pump pulse will steer the medium along the cooling branch of the temperature hysteresis. In this case, the dynamics will not depend on how the medium was brought in the very first initial state. Moreover, there is a finite probability that after each pump-induced heating the medium relaxes to one or another metastable state. The temperature dependence of the THz emission shown in Fig.3 indicates that the probability of the relaxation to each of the two stable states is 50%.

It is known that a moderate magnetic field and a relatively narrow range of temperature change

should not affect the timescale of ultrafast laser-induced demagnetization of metallic ferromagnets [22]. At the same time, launching a phase transition from an AF to a FM phase will generate ferromagnetic nuclei with random orientations [21] of their magnetizations and the speed with which the magnetizations will be aligned along the applied magnetic field should be a function of the magnetic field and temperature [21,23,24]. Therefore, the fact that the THz spectra are neither influenced by temperature nor magnetic field suggests that the origin of the THz emission is the vertical spincurrent across the FeRh/Pt interface, due to an ultrafast demagnetization of already present FM FeRh domains. Furthermore, we measured the laser-induced E_Y -THz emission in a thinner stack of MgO/FeRh(20 nm)/Pt(5 nm). Figure 5 shows the comparison of the E_Y -THz electric field signals measured in MgO/FeRh(20 nm)/Pt(5 nm) and MgO/FeRh(40 nm)/Pt(5 nm) samples. It is seen that when the magnetic layer thickness is reduced by half, the E_Y -THz peak-to-peak value that is proportional to the degree of ultrafast demagnetization is reduced by about 50%. This finding strengthens our argument that the observed E_Y -THz emission corresponds to the bulk spin-to-charge conversion of laser-induced spin currents in FeRh/Pt rather than an interface effect [33].

Recently, it has been shown that the generation of a backflow charge current from a ferromagnet/dielectric interface by femtosecond laser excitation and its subsequent conversion into a transverse transient charge current via the anomalous Hall effect (AHE), leads to an emission of THz radiation [31,32]. One may argue that the observed E_Y -THz emission in our experiments could also be due to a backflow of the laser-induced spin currents at the MgO/FeRh and FeRh/Pt interfaces, and their subsequent conversion into a net transverse charge current due to the AHE in FeRh. In this case one would expect almost no difference in the strengths of the E_Y -THz electric fields measured in FeRh for different capping layers. Our recent study (see Supplementary Material of Ref.[34]) has shown that for MgO/FeRh/Pt and MgO/FeRh/Au bilayers the amplitude of the E_Y -THz from FeRh/Pt is much larger compared to that from FeRh/Au. This is attributed to the effective spin-to-charge conversion in Pt [10,11] that has a larger spin-Hall angle compared to Au, suggesting that the observed E_Y -THz signals are mainly due to the ISHE rather than the AHE in FeRh itself.

Changing the polarization of the detected THz electric field, our experimental setup becomes sensitive to a different source of the radiation. Supplementary Material Fig.S3a shows the time traces of the THz electric field along the x-axis (E_x) obtained at $T = 450$ K for the cases corresponding to pumping the sample from the side of the Pt-layer or the MgO-substrate, respectively. The sign change shows that the source of the radiation is of electric dipole origin. Changing the helicity of the pump or changing the polarity of the applied magnetic field also results in helicity dependence of the E_x -field (see Supplementary Material Fig.3b,c). The symmetry of the experiments is in agreement with the mechanism discovered for Pt/Co bilayers [9], where circularly polarized light exerted a torque on the magnetization of Co due to the inverse Faraday effect [27], thereby tilting it in the sample plane. This tilt resulted in an electric current at the Pt/Co interface due to the inverse spin-orbit torque effect [28,29]. The peak values of the THz E_x -field extracted from the curves shown in Fig.2b, are also plotted in Fig.3. It is seen that the E_x -field follows the same dependence as the E_Y -field, showing the lack of temperature hysteresis and revealing the fact that photo-induced spin currents at the FeRh/Pt interface increase with the growth of the FM phase in FeRh. Finally, the Fourier spectra of the E_x and E_Y -electric fields (for $T = 450$ K, and $B = 150$ mT) are presented in Fig. 4c. The shift in the peak THz frequencies indicates the different sources of the laser-induced femtosecond photocurrents at an FeRh/Pt interface responsible for these signals. The observed shift in the Fourier spectrum of the E_x -THz electric field towards the higher frequency side indicates that the laser-induced tilting of the net magnetization occurs faster than the laser-induced ultrafast demagnetization. While the effective laser-induced magnetic field that tilts the magnetization due to inverse Faraday effect is present only during the action of the femtosecond laser pulse and can be essentially seen as an instantaneous process [27], ultrafast laser-induced demagnetization is not instantaneous and evolves on a time scale longer than the pulse duration [30].

To conclude, we discussed the potential explanations for the absence of the temperature hysteresis near first order magnetic phase transition in FeRh when probed with time-resolved THz spectroscopy. We revealed two different spin-dependent sources of laser-induced THz emission in an FeRh/Pt bilayer. The

most intense source originates from ultrafast laser-induced demagnetization of ferromagnetic FeRh and the inverse spin-Hall effect in the Pt-film. The second, weaker, source of THz emission is due to photo-induced magnetization tilting and the inverse spin-orbit torque at the FeRh/Pt interface.

SUPPLEMENTARY MATERIAL

See supplementary material for the schematic of the experimental setup used, and also for the data corresponding to the electric dipole origin of E_{γ} -THz emission and helicity dependence in E_{γ} -THz emission.

ACKNOWLEDGEMENT

Support for this research was from the U. S. Department of Energy Grant No. DE-SC0018237, the Nederlandse Organisatie voor Wetenschappelijk Onderzoek (NWO), the European Union Horizon 2020 and innovation program under the FET-Open grand agreement no.713481 (SPICE), the European Research Council ERC grant agreement no.856538 (3D-MAGiC), and grant agreement 852050

References:

- 1) V. Baltz, A. Manchon, M. Tsoi, T. Moriyama, T. Ono, and Y. Tserkovnyak, *Rev. Mod. Phys.* **90**, 015005 (2018).
- 2) P. Němec, M. Fiebig, T. Kampfrath, and A. V. Kimel, *Nature Physics* **14**, 229 (2018).
- 3) J. Walowski and M. Münzenberg, *J. Appl. Phys.* **120**, 140901 (2016).
- 4) L. H. Lewis, C. H. Marrows, and S. Langridge, *J. Phys. D: Appl. Phys.* **49**, 323002 (2016).
- 5) Jan-Ulrich Thiele, Stefan Maat, Member, J. Lee Robertson, and Eric E. Fullerton, *IEEE Transactions on Magnetics* **40**, 2537 (2004).
- 6) Y. Wang, M. M. Decker, Th. N.G. Meier, X. Chen, Ch. Song, T. Grünbaum, W. Zhao, J. Zhang, L. Chen, and C. H. Back, *Nature Comm.* **11**, 275 (2020).
- 7) T. Seifert, U. Martens, S. Günther, M. A. W. Schoen, F. Radu, X. Z. Chen, I. Lucas, R. Ramos, M. H. Aguirre, P. A. Algarabel, A. Anadón, H. S. K. Korner, J. Walowski, C. Back, M. R. Ibarra, L. Morellón, E. Saitoh, M. Wolf, C. Song, K. Uchida, M. Münzenberg, I. Radu and T. Kampfrath *SPIN* **7**, 3 (2017).

(MAGSHAKE) is greatly acknowledged. Authors want to thank Ray Descoteaux from CMRR, and Sergey Semin, Tonnie Toonen, and Chris Berkhout from Radboud University for all the technical support.

DATA AVAILABILITY

The data that supports the findings of this study are available within the article [and its supplementary material].

- 8) M. Battiato, K. Carva, and P. M. Oppeneer, *Phys. Rev. B* **86**, 024404 (2012).
- 9) D. M. Nenko, B. Rethfeld, and H. C. Schneider, *Phys. Rev. B* **98**, 224416 (2018).
- 10) T. Seifert, S. Jaiswal, U. Martens, J. Hannegan, L. Braun, P. Maldonado, F. Freimuth, A. Kronenberg, J. Henrzi, I. Radu, E. Beaurepair, Y. Mokrousov, P. M. Oppeneer, M. Jourdan, G. Jakob, D. Turchinovich, L. M. Hayden, M. Wolf, M. Münzenberg, M. Klaui, and T. Kampfrath, *Nat. Photonics* **10**, 483 (2016).
- 11) T. J. Huisman, R. V. Mikhaylovskiy, J. D. Costa, F. Freimuth, E. Paz, J. Ventura, P. P. Freitas, S. Blügel, Y. Mokrousov, Th. Rasing and A. V. Kimel, *Nature Nanotechnology* **11**, 455 (2016).
- 12) R. Fan, C. J. Kinane, T. R. Charlton, R. Dorner, M. Ali, M. A. de Vries, R. M. D. Brydson, C. H. Marrows, B. J. Hickey, D. A. Arena, B. K. Tanner, G. Nisbet, and S. Langridge, *Phys. Rev. B* **82**, 184418 (2010).
- 13) F. Pressacco, V. Uhlíř, Matteo Gatti, Azzedine Bendouna, Eric, E. Fullerton, and Fausto Sirotti, *Sci. Rep.* **6**, 22383 (2016).
- 14) C. Gatel, B. Warot-Fonrose, N. Biziere, L. A. Rodríguez, D. Reyes, R. Cours, M. Sastiella,

- and M. J. Casanove, Nat. Commun. **8**, 15703 (2017).
- 15) T. Kampfrath, M. Battiato, P. Maldonado, G. Eilers, J. Notzold, S. Mahrlein, V. Zbarsky, F. Freimuth, Y. Mokrousov, S. Blügel, M. Wolf, I. Radu, P. M. Oppeneer and M. Münzenberg, Nature Nanotechnology **8**, 256 (2013).
 - 16) B. F. Miao S.Y. Huang, D. Qu, and C. L. Chien, Phys. Rev. Lett. **111**, 066602 (2013).
 - 17) G. Ju, J. Hohlfeld, B. Bergman, R. J. M. van deVeerdonk, O. N. Mryasov, J.-Y. Kim, X. Wu, D. Weller, and B. Koopmans, Phys. Rev. Lett. **93**, 197403 (2004).
 - 18) J.-U. Thiele, M. Buess, and C. H. Back, Appl. Phys. Lett. **85**, 2857 (2004).
 - 19) M. Menarini, R. Medapalli, E. E. Fullerton, and V. Lomakin, AIP Advances **9**, 035040 (2019).
 - 20) S. Günther, C. Spezzani, R. Ciprian, C. Grazioli, B. Ressel, M. Coreno, L. Poletto, P. Miotti, M. Sacchi, G. Panaccione, V. Uhlir, E. E. Fullerton, G. De Ninno, and C.H. Back, Phys. Rev. B **90**, 180407(R) (2014).
 - 21) B. Bergman, Ganping Ju, Julius Hohlfeld, René J. M. van de Veerdonk, Jai-Young Kim, Xiaowei Wu, Dieter Weller, and Bert Koopmans Phys. Rev. B **73**, 060407 R (2006).
 - 22) E. Beaurepaire, J.-C. Merle, A. Daunois, and J.-Y. Bigot, Phys. Rev. Lett., **76**, 4250 (1996).
 - 23) J. A. de Jong, A. V. Kimel, R. V. Pisarev, A. Kirilyuk, and Th. Rasing, Phys. Rev. B **84**, 104421 (2011).
 - 24) D Afanasiev, B. A. Ivanov, A. Kirilyuk, T. Rasing, R. V. Pisarev, A. V. Kimel, Phys. Rev. Lett. **116**, 097401 (2016).
 - 25) G Li, R Medapalli, R.V. Mikhaylovskiy, F.E. Spada, Th. Rasing, E.E. Fullerton, A.V. Kimel, Phys. Rev. Materials **3**, 084415 (2019).
 - 26) E. Beaurepaire, M. Maret, V. Halte, J.-C. Merle, A. Daunois, and J.-Y. Bigot, Phys. Rev. B **58**, 12134 (1998).
 - 27) A. V. Kimel, A. Kirilyuk, P. A. Usachev, R. V. Pisarev, A. M. Balbashov, and Th. Rasing, Nature (London) **435**, 655 (2005).
 - 28) A. Manchon and S. Zhang Phys. Rev. B **79**, 094422 (2009).
 - 29) K. I. M. Miron, C. O. Avci, F. Freimuth, Y. Mokrousov, S. Blügel, S. Auffret, O. Boulle, G. Gaudin, and P. Gambardella, Nature Nanotechnology **8**, 587–593 (2013).
 - 30) L. Guidoni, E. Beaurepaire, and J.-Y. Bigot, Phys. Rev. Lett. **89**, 017401 (2002).
 - 31) Q. Zhang, Z. Luo, H. Li, Y. Yang, X. Zhang, and Y. Wu, Phys. Rev. Appl. **12**, 054027 (2019).
 - 32) Y. Wu, M. Elyasi, X. Qiu, M. Chen, Y. Liu, L. Ke, H. Yang, Adv. Mater. **29**, 1603031 (2017).
 - 33) X. Wang, L. Cheng, D. Zhu, Y. Wu, M. Chen, Y. Wang, D. Zhao, C.B. Boothroyd, Y.M. Lam, J.-X. Zhu, et al., Adv. Mater. **30**, 1802356 (2018).
 - 34) G. Li, R. Medapalli, J. Mentink, R. V. Mikhaylovskiy, S. K. K. Patel, A. K. Zvezdin, Th. Rasing, E. E. Fullerton, and A. V. Kimel, *under review*, Phys. Rev. Lett.

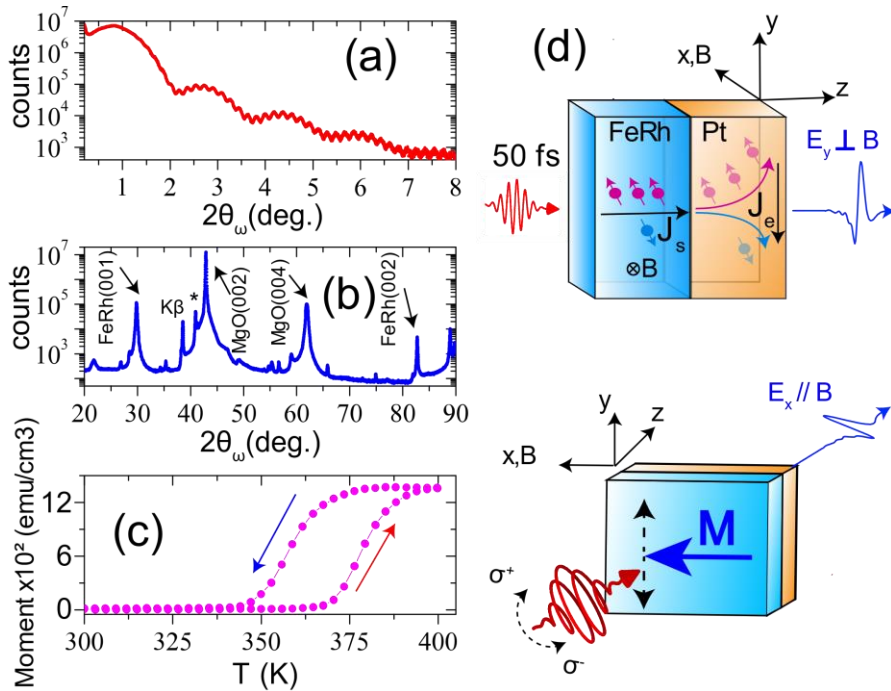


Fig. 1. (a) X-ray reflectometry and (b) x-ray diffraction spectra measured in MgO/FeRh(40 nm)/Pt(5 nm). (c) The net magnetic moment of the 40 nm-thick FeRh sample measured with an in-plane magnetic field of $B = +150$ mT. (d) Illustrations of the laser-induced femtosecond photocurrents generated by (top) the inverse spin-Hall effect in Pt (vertical spin-pumping) and (bottom) the inverse spin-orbit torque.

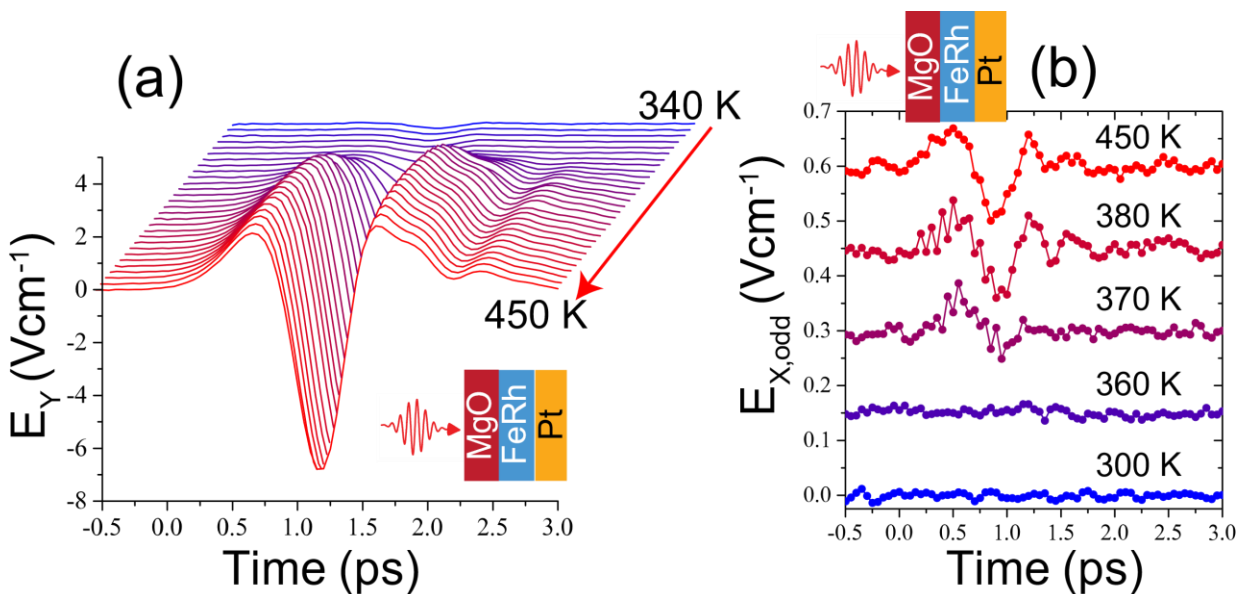


Fig. 2. (a) Time traces of the E_Y -THz electric field emission from MgO/FeRh(40 nm)/Pt(5 nm) for various initial temperatures of the sample between 300-450 K. (b) same as (a) but for the $E_{X,odd}$ -THz emission.

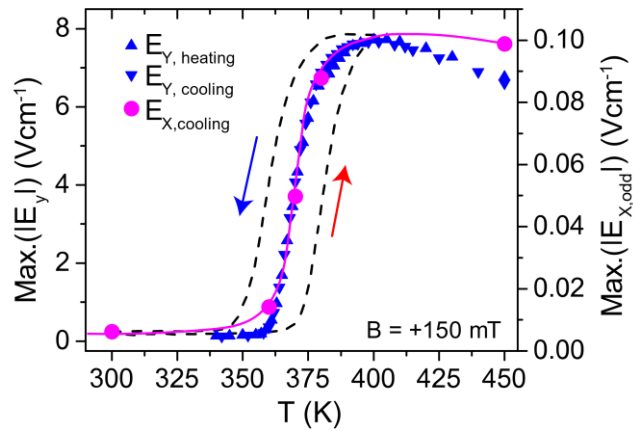


Fig. 3. The $Max.(|E_x|)$ and $Max.(|E_y|)$ as a function of T . Note that the $Max.(|E_y|)$ are shown for both sample heating and cooling processes. The magenta solid curve is a guide to the eye for the $Max.(|E_x|)$ vs T data. The magnetic moments measured with VSM are shown as dashed black curves. The red and blue arrows correspond to the heating and cooling processes. The E_X -THz data was collected for the cooling cycle case.

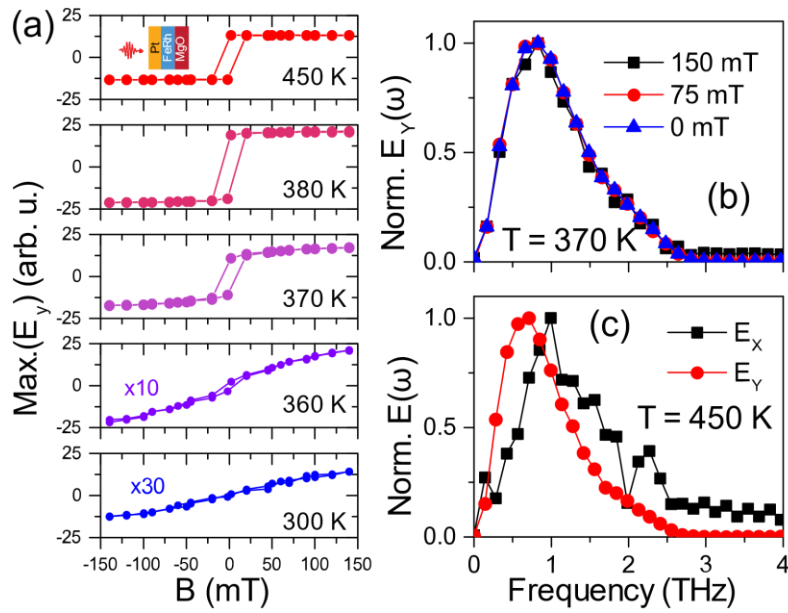


Fig. 4. (a) The $\text{Max}(|E_y|)$ as a function of the magnetic field for various initial sample temperatures between 300 and 450 K. Note that the measurements were done during the cooling process. (b) Fourier spectra of the THz waveforms measure at $T = 370$ K for three different values of B . (c) The comparison of Fourier spectra for E_x and E_y -THz electric fields detected at $T = 450$ K with $B = +150$ mT.

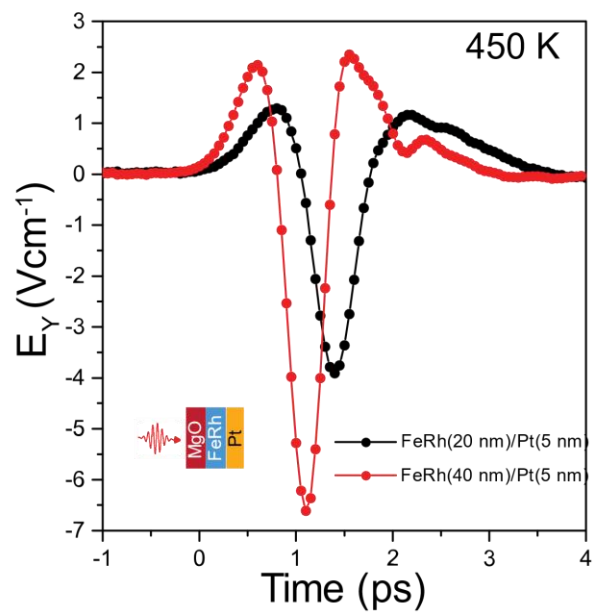


Fig. 5. Time traces of the E_Y -THz emission from (black) MgO/FeRh(20 nm)/Pt(5 nm) and (red) MgO/FeRh(40 nm)/Pt(5 nm). The measurements were done for the case of $T = 450$ K with saturation along M^I .